# Microwave Radiometry of Atmospheric Precipitation: Radiative Transfer Simulations with Parallel Supercomputers.

Yaroslaw Ilyushin[1,2] ✉ and Boris Kutuza[2]

[1] Moscow State University, Physical Faculty 119992 GSP-2 Moscow Russia
`ilyushin@phys.msu.ru`
[2] Kotel'nikov Institute of Radio Engineering and Electronics, Russian Academy of Sciences, Moscow, 125009, Russia `kutuza@cplire.ru`

**Abstract.** In the present paper, the problems of formation and observation of spatial and angular distribution of thermal radiation of raining atmosphere in the millimeter wave band are addressed. Radiative transfer of microwave thermal radiation in three-dimensional dichroic medium is simulated numerically using high performance parallel computer systems. Governing role of three dimensional cellular inhomogeneity of the precipitating atmosphere in the formation of thermal radiation field is shown.

**Keywords:** Microwave radiometry, precipitation, radiative transfer

## 1  Introduction.

Investigation of atmospheric precipitation with space borne instrumental observations (see the Fig. 1) is one of most important problems in remote sensing. The possibility of retrieving rain intensity from microwave observations was demonstrated in 1968 with the results of Cosmos-243 space-borne experiment [1]. Rain precipitation zones over the sea were identified and rain intensity was estimated from radio brightness temperatures at wavelengths 0.8, 1.35 and 3.2 cm.

Further development of techniques of space-borne precipitation observations was related to the DMSP satellite with the microwave radiometer SSM/I [2] on board, operating in the wavelength band 0.35 – 1.6 cm. Precipitation zones have been determined as low radio brightness areas at 0.35 cm wavelength because of high single scattering albedo of big rain droplets. Also, microwave radiometry of rain precipitation has been performed from the TRMM satellite. At present, the GPM (Global Precipitation Mission) project is under development.

Due to this and other directions of research, the interaction of microwave radiation with precipitation and clouds of various types is now extensively studied [3, 4]. Many of them consist of non-spherical particles, having prevalent orientation like falling raindrops. In contrast to macroscopically isotropic media, in these media dichroism plays a key role in the generation and propagation of the radiation. These effects together with spatial inhomogeneity of the medium and

2      Ilyushin Ya., Kutuza B.

underlying surface require consideration of radiation fields in three-dimensional inhomogeneous dichroic media.

The flat layered medium model, which has been widely used for simulations during long time, is now well studied and developed [5–8]. However, it does not completely describe radiative fields in spatially inhomogeneous atmospheric precipitation. Understanding of impact of the three-dimensional effects on the microwave radiative transfer (RT) is critically important for correct interpretation of the passive radiometric measurements.

Three-dimensional RT codes were first applied to the microwave atmospheric studies [9]. Since that, there have been several published studies considering microwave RT in space-borne remote sensing, and how it is effected by inhomogeneity [3] and dichroism [6].

However, to the authors' knowledge, only a very few numerical studies of vectorial RT in three dimensional anisotropic scattering media are published [4]. This paper is motivated by the need for theoretical assessments of intensity and polarization of thermal radiation of rain precipitation, observed by a space-borne microwave radiometer. The focus of the present study is on rain instead of cloud ice mostly studied by [4]. This work also differs from [4] in that it was largely an algorithm comparison study focused on ground based viewing geometry of rain, rather than space-borne one. In addition, several different wavelengths are used in simulations to investigate capabilities of multi-spectral radiometry for retrievals of rain intensity.
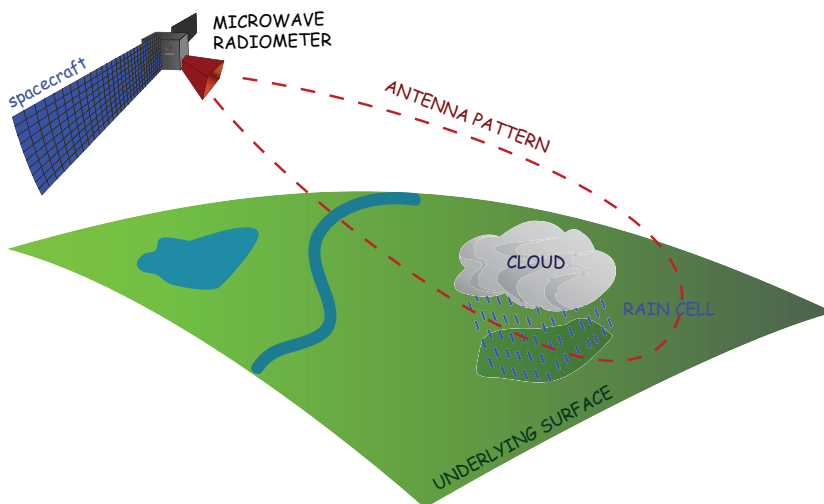


**Fig. 1.** Schematic view of the space-borne radiometry experiment.

## 2  Physical model of radiative characteristics of the medium.

In the present study, two models of raining atmosphere (uniform flat layer and three dimensional cubic rain cell) are investigated and compared.

In the rain cell model, the contribution of vertical side walls in radiative balance between the cell and surrounding medium is essential. Following to [4], we chose a cubic rain cell model ($3 \times 3 \times 3$km ), uniformly filled with falling raindrops. These dimensions are close to the typical size of realistic rain cells [10] and characteristic scales of spatial inhomogeneity in stochastic RT models in rain [11].

Physical (thermodynamic) temperature in the atmosphere is non-uniform and decreases with height $T_2 = (300 - 7z)\,K$, where $z$ is a height in km.

The underlying surface (Fig. 2) is approximated with a horizontal flat nearly isotropically radiating gray surface with partial lambertian reflection. Thermal radiative emission of the heated underlying surface is slightly vertically polarized [12]. In the millimeter wave band, this model provides a reasonable approximation for most terrestrial soils and vegetation covers. Radiative absorption by the liquid phase water clouds [13] and atmospheric gases is taken into account separately.

Underlying surface in the flat layer model is either black ( lambertian reflection coefficient $R = 0$) or gray ($R = 0.25$). In the cubic rain cell model, the underlying surface within the square bottom of the cell is also black or gray as well as in the uniform slab model. Outside the bottom surface, it is totally black ($R = 0$). The temperature dependence of dielectric properties of liquid water have been ignored, thus the properties of the medium have been assumed to be constant in the whole height range of the cell or the slab. All the dielectric properties of the water have been evaluated for $T = 0°C$. Accounting for the height gradient of the temperature in the problem under consideration thus reduces to the temperature dependence of the Planck function in the RT equation and boundary conditions on the rain cell side walls.

Complex dielectric permittivity of the liquid water obeys the Debye formula [14]

$$\varepsilon = \varepsilon_0 + \frac{\varepsilon_s - \varepsilon_0}{1 + i\Delta\lambda/\lambda}\,, \tag{1}$$

where

$$\Delta\lambda = 2\pi\tau_p \frac{\varepsilon_s + 2}{\varepsilon_0 + 2}\,, \tag{2}$$

$\varepsilon_s$ – static dielectric permittivity of liquid water (at frequencies $\nu \ll 1/\tau_p$), $\varepsilon_0 \approx 4.9$ – optical dielectric permittivity of liquid water (at frequencies $\nu \gg 1/\tau_p$), and relaxation time

$$\tau_p = \exp\left\{9.8\left(\frac{273}{T + 273} - 0.955\right)\right\} \cdot 10^{-12}\ \text{s}\ . \tag{3}$$

4        Ilyushin Ya., Kutuza B.

The static dielectric permittivity if the liquid water is described by an approximate formula [12]

$$\varepsilon_s(T) = 88.045 - 0.4147\,T + 6.295 \cdot 10^{-4}\,T^2 + 1.075 \cdot 10^{-5}\,T^3\,. \qquad (4)$$

Geometrical model of non-spherical falling raindrops shape can be found, e.g. in [15]. With a reasonable degree of approximation falling raindrops can be regarded to be oblate spheroids with vertically oriented rotational axis of symmetry. The ratio of axes of the spheroid approximately is [5]

$$\frac{b}{a} = 1 - 0.091\bar{a}\,, \qquad (5)$$

where $\bar{a}$ – is the radius of the spherical raindrop of the equivalent volume in mm.

Raindrop sizes are distributed statistically according to Marshall-Palmer distribution [16]

$$n(\bar{a}) = N_0 \exp(-q\bar{a})\,, \qquad (6)$$

where $N_0 = 16000\,\mathrm{m^{-3}mm^{-1}}$, $q = 8.2R^{-0.21}$, $R$ – rain intensity, mm/h.

Extinction and absorption matrices of the spheroidal particles of fixed orientation can be evaluated by publicly available T-matrix codes [17].

Thus, radiative properties of the rain precipitation medium (volume extinction and absorbtion matrices) were evaluated within the physical model formulated above. Obtained radiative properties are close to those evaluated in [18, 4]. It can be seen that the volume extinction coefficient decreases with the increase of the wavelength. Simultaneously, single scattering albedo decreases, which is in qualitative agreement with the known results for the small absorbing particles (in clouds). In addition, the longer the wavelength, the more pronounced is dichroism (difference of the absorption and extinction between the horizontal and vertical polarization).

## 3    Radiative transfer in the anisotropic scattering medium.

Spatial and angular distribution of the intensity and polarization of thermal radiation in the rain precipitation medium is governed by the vectorial radiative transfer equation

$$(\boldsymbol{\Omega} \cdot \nabla)\mathbf{I}(\boldsymbol{r}, \boldsymbol{\Omega}) = -\hat{\sigma}_\varepsilon \mathbf{I}(\boldsymbol{r}, \boldsymbol{\Omega}) + \bar{\sigma}_a B_\lambda(T_2(z)) + \frac{1}{4\pi}\int\limits_{4\pi} \hat{x}(\boldsymbol{\Omega}, \boldsymbol{\Omega}')\mathbf{I}(\boldsymbol{r}, \boldsymbol{\Omega}')d\boldsymbol{\Omega}'\,, \;(7)$$

where $\boldsymbol{\Omega} = (\mu_x, \mu_y, \mu_z)$ – unit vector of arbitrary direction, $\mathbf{I}(\mathbf{z}, \boldsymbol{\Omega}) = \{I, Q, U, V\}$ – Stokes parameters vector of polarized radiation, $\hat{\sigma}_\varepsilon = \hat{\sigma}_\varepsilon(\boldsymbol{\Omega})$ – extinction matrix of polarized radiation in the medium, $\bar{\sigma}_a$ – vector of true absorption in the medium, $\hat{x}(\boldsymbol{\Omega}, \boldsymbol{\Omega}')$ – scattering matrix, $B_\lambda(T)$ – Planck black body radiation function. Formulae for evaluation of the true absorption vector components $\bar{\sigma}_a$ can be found, e.g., in [16].

In the millimeter wave band at temperatures about $300\,K$, typical for lower terrestrial atmosphere, Planckian black body radiation at the given wavelength is roughly proportional to the black body temperature (Rayleigh-Jeans law). This allows the Stokes parameters to be expressed immediately through the equivalent black body temperature (radio brightness temperature).

Boundary problem for the vectorial radiative transfer equation in three dimensional cubic rain cell consists of the equation (7) and boundary conditions for the incoming radiation at bottom and top sides of the cubic cell, respectively, and boundary conditions at the side walls of the cube. Boundary condition on the top surface of the rain cell is just zero boundary condition for the incoming radiation. Boundary conditions on side walls and bottom of the rain cell account for the thermal radiation coming from the heated underlying surface and lossy gray surrounding atmosphere. For their exact fomulation the reader is referred to [19].
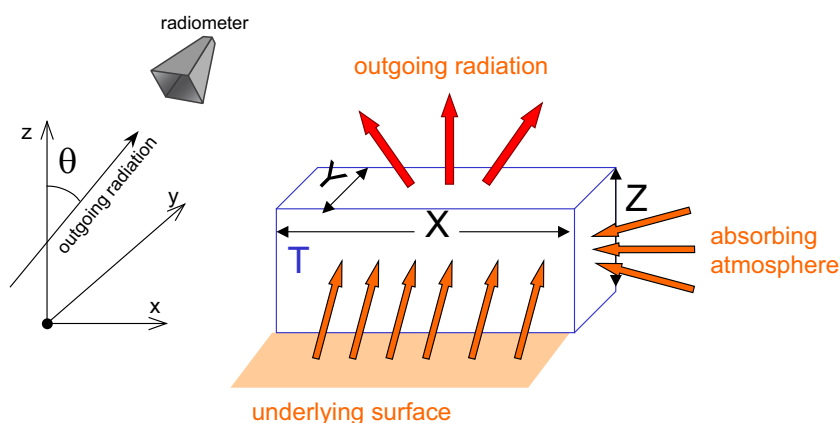


**Fig. 2.** Schematic view of the rain cell model geometry.

## 4   Radiative transfer equation in three dimensional rain cell.

The boundary problem for the vectorial radiative transfer equation in a three dimensional cubic rain cell consists of the equation (7)and boundary conditions for the incoming radiation on the bottom and top sides of the cubic cell, and boundary conditions at the side walls of the cube. Boundary conditions on the top and bottom sides of the cube are

$$\mathbf{I}(0, \boldsymbol{\Omega} \cdot \mathbf{z} > 0) = \{2T_1 + 2T_D, Q_1, 0, 0\},\tag{8}$$

$$\mathbf{I}(z_0, \boldsymbol{\Omega} \cdot \mathbf{z} < 0) = \{0, 0, 0, 0\},\tag{9}$$

6       Ilyushin Ya., Kutuza B.

where $\mathbf{z}$ – unit vector of positive direction of $z$ axis, $T_1$ and $Q_1$– radio brightness temperature and polarization of the underlying surface emission, $T_D$ – radio brightness temperature of diffuse reflection from the underlying surface, defined by an equation

$$T_D \int\limits_0^1 \mu\,d\mu = -R \int\limits_{-1}^0 T(\mu)\mu\,d\mu \tag{10}$$

at $z = 0$.

Boundary conditions on the side walls determine intensity and polarization of the radiative fluxes, incident on the wall of the cube from the underlying surface and heated absorbing atmosphere, surrounding the cell from side directions, as is schematically shown in the Fig. 3. If the physical temperature of the atmosphere is stratified vertically, fluxes going up consist of attenuated thermal radiation coming from the periphery of the underlying surface and thermal radiation of the atmosphere itself,

$$I(Z) = I_1(0) \exp\left(-\int\limits_0^Z \frac{\kappa dz}{\mu_z}\right) + \int\limits_0^Z 2T_2(z)\kappa \exp\left(-\int\limits_z^Z \frac{\kappa dz'}{\mu_z}\right) dz\,, \tag{11}$$

$$Q(Z) = Q_1(0) \exp\left(-\int\limits_0^Z \frac{\kappa dz}{\mu_z}\right)\,, \tag{12}$$

where $\kappa$ is the volume extinction coefficient in the surrounding atmosphere. Corresponding fluxes going down consist of the atmospheric thermal radiative emissions only

$$I(Z) = \int\limits_{z_0}^Z 2T_2(z)\kappa \exp\left(-\int\limits_z^Z \frac{\kappa dz'}{\mu_z}\right) dz\,, \tag{13}$$

$$Q(Z) = 0\,. \tag{14}$$

Horizontal fluxes, incident on the side walls of the cube, are

$$I(Z) = 2T_2(Z)\,, \tag{15}$$

$$Q(Z) = 0\,. \tag{16}$$

For linear dependence of the atmospheric temperature $T_2$ from the height

$$T_2(z) = T_2(0) + gradT_2 \cdot z\,, \tag{17}$$

the formulae given above yield explicit expressions, convenient for practical usage in computer simulations.
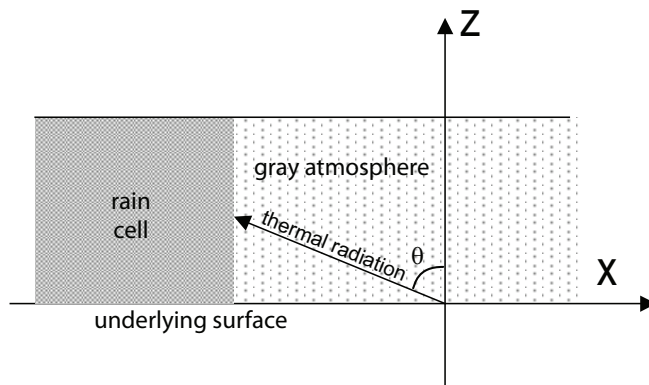
**Fig. 3.** To the formulation of the side wall boundary condition for the rain cell model.

The vectorial radiative transfer equation was solved by the DO method. Corresponding discretized three dimensional equation is

$$\mu_{xi}\frac{\partial}{\partial x}\mathbf{I}_i + \mu_{yi}\frac{\partial}{\partial y}\mathbf{I}_i + \mu_{zi}\frac{\partial}{\partial z}\mathbf{I}_i = -\hat{\sigma}_\varepsilon \mathbf{I}_i + 2\pi \sum_{l,j} x(\boldsymbol{\Omega}_i, \boldsymbol{\Omega}_j)a_j \mathbf{I}_j + SF_i(z) , \quad (18)$$

where $\boldsymbol{\Omega}_i = \{\mu_{xi}, \mu_{yi}, \mu_{zi}\}$ is a unit vector of direction of $i - $ th node of the quadrature formula.

In practice, observed radiometric data are in fact a convolution of the observed radiation field with the receiving antenna pattern of the instrument. [20] concluded that inhomogeneity effects could be largely explained by the beam-filling effect, which is essentially a straightforward consequence of averaging over radiances that have a non-linear response to hydrometeors. In [21] this was also demonstrated for polarized RT by comparison with the independent pixel approximation. However, the footprint size of the space-borne microwave radiometer [22–25] is notably larger than typical size of the rain cell [10]. For this reason, averaged contribution of rain cell in the registered radio brightness temperature can be well approximated by an integral over the whole projection area of the top and two side surfaces of the cube, as is shown in the Figure 2:

$$\bar{\mathbf{I}}(\boldsymbol{\Omega}) = \frac{\underset{(1)}{\int} \mathbf{I}(x,y,Z,\boldsymbol{\Omega})\mu_z\,dxdy + \underset{(2)}{\int} \mathbf{I}(X,y,z,\boldsymbol{\Omega})\mu_x\,dzdy + \underset{(3)}{\int} \mathbf{I}(x,Y,z,\boldsymbol{\Omega})\mu_y\,dxdz}{\underset{(1)}{\int} \mu_z\,dxdy + \underset{(2)}{\int} \mu_x\,dzdy + \underset{(3)}{\int} \mu_y\,dxdz} =$$

$$= \frac{\underset{(1)}{\int} \mathbf{I}(x,y,Z,\boldsymbol{\Omega})\mu_z\,dxdy + \underset{(2)}{\int} \mathbf{I}(X,y,z,\boldsymbol{\Omega})\mu_x\,dzdy + \underset{(3)}{\int} \mathbf{I}(x,Y,z,\boldsymbol{\Omega})\mu_y\,dxdz}{XY\mu_z + XZ\mu_y + YZ\mu_x} , \quad (19)$$

where the indices (1),(2) and (3) denote integration over the top and two side surfaces of the rectangular cell, respectively, $X, Y, Z$ are horizontal dimensions of the cell. For the cubic cell, which is considered here, $X = Y = X = 3\,\mathrm{km}$.

8       Ilyushin Ya., Kutuza B.

Assuming typical values of total water vapor and liquid water content 2 g/cm$^2$ and 0.5 kg/m$^2$, respectively, and accounting for the absorption by the molecular oxygen [19], additional absorption coefficients 0.33, 0.066 and 0.013 $km^{-1}$ for wave lengths 3, 8 and 22.5 mm have been assumed for simulations. These values are relatively small and do not play significant role in millimeter wave band thermal radiation field of rain, except of the weakest ones (less than several mm/h)

## 5    Simulation results.

The set of simultaneous differential equations (18) together with the proper discretized boundary conditions for all the sides of the cubic cell has been solved by the finite difference (FD) scheme (upwind differences [26]) by iterative convergence to the stationary regime. Scattering integral has been approximated by the Gaussian spherical quadrature formula of 29th order G29 [27] with 302 discrete ordinates.

Numerical algorithm was implemented and run on parallel computers "Tshchebyshev" and "Lomonosov" of the Scientific and Research Computing Center of the Moscow State University [28] with C++ programming language. Cyclically repeated calculations of the iteration scheme were parallelized with OpenMP parallel computing standard. Each scenario, dependent of rain intensity and the wave length, has been simulated on a separate individual node of the parallel cluster. That means, 8 or 12 processing cores were allocated for each scenario. On the nodes with processors supporting hyper-threading technology (HTT), it corresponds to 16 or 24 threads, respectively. Size of memory and number of computing cores of each individual node of both parallel clusters allowed for fully polarized radiative transfer simulations on the three-dimensional rectangular grid as large as $64 \times 64 \times 64$ nodes with $4 \times 302 = 1208$ unknown parameters at each node. Since solution in each node of the grid is updated independently at every iteration of the FD scheme, computer code parallelization requires a minimal effort, with the speedup nearly proportional to the number of processing cores. Running time limit (72 hours) allowed to run the process until it converged to the accuracy of the Stokes parameters $10^{-4}K$ uniformly over the whole three-dimensional domain.

There has been performed large series of numerical simulations of microwave RT in slab layer and rectangular rain cell with different parameters (rain intensity, additional atmospheric absorption and underlying surface diffuse reflection coefficient) [29]. Angular and spatial distributions of the intensity and polarization of the outgoing thermal radiation at different wavelength has been simulated for a number of values of rain intensity, reflectivity of underlying surface and some other parameters, which required significant computing time on parallel cluster with many nodes. Results of complete series of calculations are available from the official site of the project [30]. Typical simulated three-dimensional views of rain cell are shown in the Figures 4,5.

Distributions of the polarization parameters Q and U of the cell with absolutely black underlying surface (the Figure 4 ) do not differ significantly from the ones of partially reflective underlying surface (the Figure 5). On the other hand, the radio brightness temperature (the intensity, Stokes parameter I, the Figure 4 ) is notably impacted by the Lambertian reflectivity of the surface beneath the cell. Roughly speaking, the cold cell bottom is partially seen through the cell's side walls.
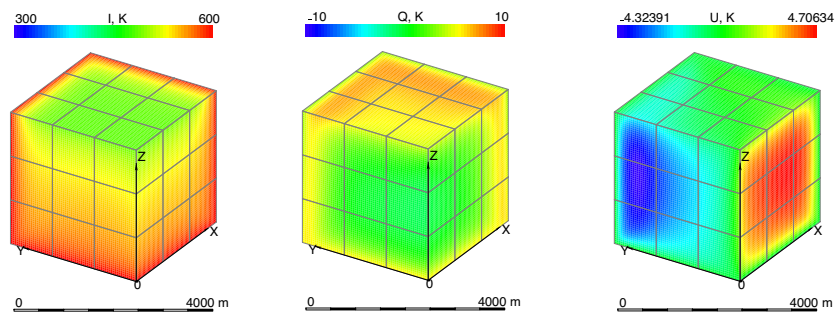


**Fig. 4.** (Color online) 3D rain cell view projection. Wave length $\lambda = 3$ mm , rain intensity 20 mm/h, Lambertian reflectance $R = 0$.
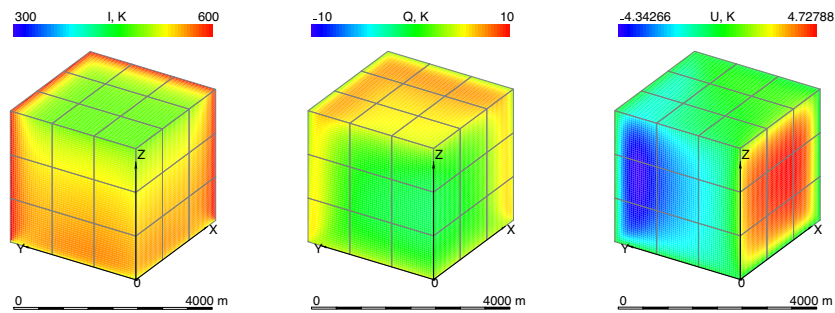


**Fig. 5.** (Color online) 3D rain cell view projection. Wave length $\lambda = 3$ mm , rain intensity 20 mm/h, Lambertian reflectance $R = 0.25$

10      Ilyushin Ya., Kutuza B.

From the simulation results it turns out that geometrical model of isolated cubic rain cell, which is rough simplification of true inhomogeneous distribution of realistic rain precipitation in the atmosphere, showed inhomogeneous distribution of thermal radiation intensity and polarization. It worth also noting appearance of the third Stokes parameter U, which is observed experimentally [31], in the simulated radiative field of the rain cell. This parameter U, which characterizes the tilt angle of the radiation polarization plane, does not appear in the layered slab medium model with the vertically oriented axes of the rotationally symmetric particles (raindrops). The polarization plane of the thermal radiation of layered slab medium can be tilted, if the rotational axes of the raindrops are systematically tilted themselves [31]. The mechanisms of such raindrops' axes inclination (wind etc.) are, however, still questionable, and are out of the scope of this paper. The rain cell model is therefore able to qualitatively explain the polarization plane tilt without the tilted raindrops hypothesis being involved.

Thus, RT simulations with the cubic cell model discovered limitations of flat layered slab model, which still largely remains the basic and most used computational model in atmospheric radiation studies.

## 6     Conclusions and final remarks.

In the study presented here, extensive numerical simulations of thermal radiation field in precipitating atmosphere in millimeter wave band have been performed. Commonly used uniform slab model of rain atmosphere is validated against three-dimensional rain cell model. Simulation results for intensity and polarization of the thermal radiation have been presented and interpreted.

Obtained results can appear to be helpful for interpretation of space-borne microwave radiometry observational data. Calculations confirm linear polarization of rain cell thermal radiation, which is about 2-3 K in average over observable surface area of the cell.

Spatial resolution of existing space-borne millimeter wave radiometers is now about 15-20 km, which well exceeds typical size of the rain cell. Thus, several rain cells with different rain intensity are typically covered by the radiometer's field of view. Because of large contribution of underlying surface to the intensity and polarization, it is not possible to separate it from the contribution of precipitation (rain). To do that, one needs to improve significantly spatial resolution of the radiometer, to make its field of view comparable to or smaller than typical rain cell dimension. This can be acheived with millimeter wave synthetic aperture interferometer, or with large size antenna systems with capability of electrical or mechanical scanning.

## Acknowledgements.

# References

1. Basharinov, A.E., Gurvich, A.S., Egorov, S.T.: Radio Emission of the Earth as a Planet. Nauka, Moscow (1974)

2. Spencer, R., Goodman, H., Hood, R.: Precipitation retrieval over land and ocean with the SSM/I: Identification and characteristics of the scattering signal. J. Ocean. Technol. **6** (1989) 254–273

3. Roberti, L., Haferman, J., Kummerow, C.: Microwave radiative transfer through horizontally inhomogeneous precipitating clouds. Journal of Geophysical Research **99**(D8) (1994) 16707–16718

4. Battaglia, A., Davis, C., Emde, C., Simmer, C.: Microwave radiative transfer intercomparison study for 3-D dichroic media. Journal of Quantitative Spectroscopy and Radiative Transfer **105**(1) (2007) 55–67

5. Evtushenko, A.V., Zagorin, G., Kutuza, B.G., Sobachkin, A., Hornbostel, A., Schroth, A.: Determination of the Stokes vector of the microwave radiation emitted and scattered by the atmosphere with precipitation. Izvestiya - Atmospheric and Ocean Physics **38**(4) (2002) 470–476

6. Emde, C., Buehler, S.A., Davis, C., Eriksson, P., Sreerekha, T.R., Teichmann, C.: A polarized discrete ordinate scattering model for simulations of limb and nadir long-wave measurements in 1-D/3-D spherical atmospheres. Journal of Geophysical Research: Atmospheres **109**(D24) (2004) D24207.

7. Ilyushin, Y., Seu, R., Phillips, R.: Subsurface radar sounding of the Martian polar cap: radiative transfer approach. Planetary and Space Science **53**(1415) (2005) 1427 – 1436

8. Ilyushin, Y.A.: Radiative transfer in layered media: Application to the radar sounding of Martian polar ices. {II}. Planetary and Space Science **55**(12) (2007) 100 – 112

9. Weinman, J.A., Davies, R.: Thermal microwave radiances from horizontally finite clouds of hydrometeors. Journal of Geophysical Research: Oceans **83**(C6) (1978) 3099–3107

10. Begum, S., Otung, I.E.: Rain cell size distribution inferred from rain gauge and radar data in the UK. Radio Science **44**(2) (2009) RS2015.

11. Tsintikidis, D., Haferman, J.L., Anagnostou, E.N., Krajewski, W.F., Smith, T.F.: A neural network approach to estimating rainfall from spaceborne microwave data. IEEE Transactions on Geoscience and Remote Sensing **35**(5) (Sep 1997) 1079–1093

12. Ulaby, F.T., Moore, R.K., Fung, A.K.: Microwave remote sensing: Active and passive. Volume 1. Reading, MA:Addison-Wesley (1981)

13. Kutuza, B.G., Smirnov, M.T.: The influence of clouds on the radio-thermal radiation of the ' atmosphere-ocean surface' system. Issledovanie Zemli iz Kosmosa **1**(3) (1980) 76–83

14. Basharinov, A.E., Kutuza, B.G.: Determination of temperature dependence of the relaxation time of water molecules in clouds and possibilities for assessing the effective temperature of drop clouds by uhf radiometric measurements. Izv. Vyssh. Uchebn. Zaved., Radiofiz. **17**(1) (1974) 52–57

12        Ilyushin Ya., Kutuza B.

15. Czekala, H., Havemann, S., Schmidt, K., Rother, T., Simmer, C.: Comparison of microwave radiative transfer calculations obtained with three different approximations of hydrometeor shape. Journal of Quantitative Spectroscopy and Radiative Transfer **63**(2-6) (1999) 545–558
16. Czekala, H., Simmer, C.: Microwave radiative transfer with nonspherical precipitating hydrometeors. Journal of Quantitative Spectroscopy and Radiative Transfer **60**(3) (1998) 365–374
17. Moroz, A.: Improvement of Mishchenko's T-matrix code for absorbing particles. Applied Optics **44**(17) (2005) 3604–3609
18. Hornbostel, A. Investigation of Tropospheric Influences on Earth-satellite Paths by Beacon, Radiometer and Radar Measurements/Doctoral Thesis (1995)
19. Ilyushin, Y.A., Kutuza, B.G.: Influence of a spatial structure of precipitates on polarization characteristics of the outgoing microwave radiation of the atmosphere. Izvestiya - Atmospheric and Ocean Physics **52**(1) (2016) 74–81
20. Kummerow, C.: Beamfilling errors in passive microwave rainfall retrievals. Journal of Applied Meteorology **37**(4) (1998) 356–370
21. Davis, C., Evans, K., Buehler, S., Wu, D., Pumphrey, H.: 3-D polarised simulations of space-borne passive mm/sub-mm midlatitude cirrus observations: A case study. Atmospheric Chemistry and Physics **7**(15) (2007) 4149–4158
22. Kutuza, B.G., Hornbostel, A., Schroth, A.: Spatial inhomogeneities of rain brightness temperature and averaging effect for satellite microwave radiometer observations. Volume 3. (1994) 1789–1791
23. Kutuza, B.G., Zagorin, G.K., Hornbostel, A., Schroth, A.: Physical modeling of passive polarimetric microwave observations of the atmosphere with respect to the third Stokes parameter. Radio Science **33**(3) (1998) 677–695
24. Kutuza, B.G., Zagorin, G.K.: Two-dimensional synthetic aperture millimeter-wave radiometric interferometric for measuring full-component Stokes vector of emission from hydrometeors. Radio Science **38**(3) (2003) 8055
25. Volosyuk, V.K., Gulyaev, Y.V., Kravchenko, V.F., Kutuza, B.G., Pavlikov, V.V., Pustovoit, V.I.: Modern methods for optimal spatio-temporal signal processing in active, passive, and combined active-passive radio-engineering systems. Journal of Communications Technology and Electronics **59**(2) (2014) 97–118
26. Richtmyer, R.D., Morton, K.W.: Difference Methods for Initial-Value Problems. Interscience Publishers, New York (1967)
27. Lebedev, V.: Quadrature formulas for a sphere of the 25–29th order of accuracy. Sib. Mat. Zh. **18**(1) (1977) 132–142
28. Sadovnichy, V.A., Tikhonravov, A., Voevodin, V., Opanasenko, V.: "lomonosov": Supercomputing at moscow state university. In: In Contemporary High Performance Computing: From Petascale toward Exascale. Chapman & Hall/CRC Computational Science, Boca Raton, USA, CRC Press (2013) 283–307
29. Ilyushin, Y.A., Kutuza, B.G.: New possibilities of the use of synthetic aperture millimeter-wave radiometric interferometer for precipitation remote sensing from space. Proceedings - 2013 International Kharkov Symposium on Physics and Engineering of Microwaves, Millimeter and Submillimeter Waves, MSMW 2013 (2013) 300–302
30. URL: http://vrte.ru/16X2014KutuzaVDO3D/testSKIF1/htmGlobal/index.html
31. Evtushenko, A., Zagorin, G., Kutuza, B., Sobachkin, A., Hornbostel, A., Schroth, A.: Determination of the Stokes vector of the microwave radiation emitted and scattered by the atmosphere with precipitation. Izvestiya - Atmospheric and Ocean Physics **38**(4) (2002) 470–476